REPORT DOCUMENTATION PAGE

Form Approved
OMB No. 0704-0188

1. REPORT DATE *(DD-MM-YYYY)*	2. REPORT ~~DATE~~ Type	3. DATES COVERED *(From - To)*
30/12/2002	Final Technical	Oct, 1999 -- Sep. 2002

4. TITLE AND SUBTITLE

Ship-Wake Scattering Calculations

5a. CONTRACT NUMBER

5b. GRANT NUMBER

N00014-00-1-0082

5c. PROGRAM ELEMENT NUMBER

6. AUTHOR(S)

James C. West

5d. PROJECT NUMBER

5e. TASK NUMBER

5f. WORK UNIT NUMBER

7. PERFORMING ORGANIZATION NAME(S) AND ADDRESS(ES)

Oklahoma State University
202 ES
Stillwater, OK 74078

8. PERFORMING ORGANIZATION REPORT NUMBER

9. SPONSORING/MONITORING AGENCY NAME(S) AND ADDRESS(ES)

Office of Naval Research
Ballston Centre Tower One, Code 334
800 N. Quincy Street
Arlington, VA 22217-5660

10. SPONSOR/MONITOR'S ACRONYM(S)

ONR

11. SPONSORING/MONITORING AGENCY REPORT NUMBER

12. DISTRIBUTION AVAILABILITY STATEMENT

APPROVED FOR PUBLIC RELEASE

20030128 203

13. SUPPLEMENTARY NOTES

14. ABSTRACT

The low-grazing-angle electromagnetic backscattering from small breaking water waves has been analyzed using computational electromagnetics (CEM) techniques. A new approach based on the multilevel fast multipole algorithm was implemented for 3-D surface crest scattering to supplement existing 2-D techniques. Multipath scattering between the wave crest and the front face can be modeled using physical optics on the face. A new method to model the specular reflection from jetting crests, termed extended gemetrical optics (EGO), was developed. The numerical calculations were shown to respond to the same measured surface features as experimental results, although polarization ratio differences demonstrate the importance of multipath scattering. Preliminary 3-D results showed that EGO may be effective in modeling the reflected from complicated jetting structures.

15. SUBJECT TERMS

Sea surface EM scattering
Rough surface EM scattering
Computational Electromagnetics

16. SECURITY CLASSIFICATION OF:			17. LIMITATION OF ABSTRACT	18. NUMBER OF PAGES	19a. NAME OF RESPONSIBLE PERSON
a. REPORT	b. ABSTRACT	c. THIS PAGE			James C. West
U	U	U	UU	16	19b. TELEPONE NUMBER *(Include area code)* 405/744-6096

Final Report
Ship-Wake Scattering Calculations
ONR Contract N00014-00-1-0082

James C. West
Oklahoma State University

Technical Objectives

The objective of the project was to facilitate the understanding and efficient modeling of microwave scattering from steep and reentrant features on the sea surface at low grazing angles (LGA). LGA sea surface scattering is characterized by brief bursts of power known as "sea spikes'' where the horizontally polarized (HH) backscatter can exceed that at vertical polarization (VV) by 10 dB or more for periods of up to a second. This behavior is not predicted by standard distributed-surface scattering models such as the Kirchhoff approximation or two-scale models which have proven accurate at moderate and large grazing-angle illumination. Sea spikes have been correlated with breaking waves in experimental studies in both laboratory wave tanks and the open sea, with maximum responses occurring at or near the time of maximum steepness of the breaking wave. The most successful models to explain sea spike responses have used fairly simple optical approaches to describe multipath scattering from the breaking crest. The differing multipath responses at the two polarizations give differing interference, leading to the sea spike. These models do not include the effects of the shape of the breaking crest on the scattered signal, nor do they include the effects of surface roughness on the multipath reflections. The primary goal of the work reported here was to identify the important scattering mechanisms in the LGA scattering from breaking waves, and to implement a general modeling approach that yields accurate prediction of the scattering cross-sections under realistic conditions.

Technical Approach

The general modeling approach for modeling the scattering from breaking waves was developed by considering the individual scattering mechanisms separately. The three mechanisms considered were the direct scattering from steep crests, the distributed-surface scattering from random roughness, and the multipath scattering between the crest and the front face of the wave. The ability of existing models to predict each mechanism was tested through comparison with reference ``exact'' scattering found using numerical electromagnetic techniques based on the moment method (MM). The individually modeled components were then combined to provide the general modeled response. The models were tested with both numerically generated surface profiles and profiles measured in laboratory wave tanks. A model for scattering in a two-dimensional environment (the surfaces are ideally uniform in a single (azimuthal) direction) was developed to give very accurate scattering cross-sections for numerically generated profiles. In this, the crest scattering is found using an MM-based approach, the multipath is found using physical optics (PO), and the distributed-surface scattering is found using the two-scale model. This model has now been applied to experimentally measured profiles. In follow-on work, work is progressing to extend this approach to arbitrary three-dimensional profiles.

The LGA scattering mechanisms were studied using computational electromagnetic techniques that provide reference "exact" scattering to which the modeled scattering can be compared. One approach is based on a hybrid technique introduced by Burnside et al. (*IEEE Trans. Antennas Propag.*, **23**, 551-558, 1975) that extends the moment method (MM) using the geometrical theory of diffraction (GTD). This approach was extended to the application to finite-conductivity rough surfaces by West et al. (*IEEE Trans. Antennas Propag.*, **46**, 93-100, 1998). This approach allows the surface to be extended infinitely with only a moderate increase in computational complexity. Thus, uniform plane wave illumination may be used, avoiding the use of an illumination weighting function that complicates the application at small grazing angles. This approach is limited to the two-dimensional scattering problem. It is being used both to find the scattering from the full surface profiles to which the model results are being compared, as well as the crest-only scattering used in the model-based results. The numerical results are also being compared directly to experimental scattering measured simultaneously with the surface profile measurements to fully validate the both the numerical and model-based 2-D approaches.

The 3-D surface calculations are much more computationally expensive than the corresponding 2-D calculations. The efficient multi-level fast-multipole algorithm (MLFMA) has been implemented to find the scattering from the crests of breaking waves in the 3-D cases. One disadvantage of any 3-D numerical EM approach is that the technique used to avoid artificial edges in the 2-D MM/GTD approach is no longer applicable. Resistive treatment is instead used to remove the effects of the edges. T MLFMA was first tested with idealized wave profiles derived from a numerically generated breakers, and then applied to 3-D wave crest profiles that were synthesized from 2-D measurements of breaker cross-sections. The calculated scattering has been compared to the predictions of different analytical scattering models.

Much of the work documented here relied upon measured surface profiles provided by Dr. James H. Duncan of the University of Maryland. The measurements were made in the University of Maryland wave tank using an optical system (Duncan *et al.*, *J. Fluid Mech.*, **379**, 191-222, 1999). Waves of approximately 1 m wavelength and varying amplitude were generated at one end of the wave tank and forced to breaking through either dispersion or side-band instability. An instrument carriage traveled with the wave crest, illuminating the crest with a laser sheet that was imaged with a video camera also mounted on the carriage. The time-evolving crest was then extracted from the individual video frames using an edge-detection procedure, yielding a continuous measurement of the 2-D cross-section of the wave to sub-millimeter resolution. These measured profiles were used here for both direct two-dimensional numerical studies, as well as to form synthetic 3-D surfaces to which the newly developed MLMFA code was applied. The availability of the detailed measured profiles allowed the testing of the numerical codes and scattering models under far more realistic conditions than previously possible.

RESULTS

Two-Dimensional Multipath Study

A two dimensional study of multipath scattering from wind-roughened breaking waves at 10 GHz (X-band) was completed. The sample surfaces used in the study were derived from samples of the time history of a plunging breaker wave that was numerically generated by researchers at the University of California-Santa Barbara using the LONGTANK computational hydrodynamic code described by (

Wang *et al.*, *Int. J. Num. Meth. Fluids*, **20**, 1315-1336, 1995). This surface series was previously treated numerically by Holliday *et al.* (*IEEE Trans. Antennas Propag.*, **46**, 108-113, 1998), who found

that a sea spike appears at a magnitude that is not predicted by the optical multipath models. The crests of the LONGTANK wave, numbered with increasing time, are shown in Figure 1. The test surfaces were obtained by isolating the section of the wave extending from behind the crest to the deepest point in the trough in front of the crest. The profiles were then rolled off and extended to infinity in planar sections to allow treatment using the 2-D hybrid MM/GTD numerical scattering code. Finally, a random roughness derived from the Pierson-Moskowitz wind-wave spectrum was added to the front face of the wave. A sample final surface derived from LONGTANK wave 9 is shown as the solid line in Figure 2.

The full surface backscattering was found by treating the crest, multipath, and distributed surface scattering separately. The crest scattering was found by isolating the crest structure from the other significant scatterers on the profile, and rolling the surface off to infinity at a steep angle. The "isolated-crest" surface is shown as the long-dashed line in Figure 2. The MM/GTD numerical scattering routine was applied to the isolated-crest profile to generate a full bistatic scattering pattern. This pattern with co-co-located incident and scattering angles gave the direct crest backscatter. The multipath scatter was found by using the bistatic crest scattering pattern to find the incident energy scattered toward the front face of the wave. The physical optics approximation was then applied to this energy, giving a surface current that was then reradiated to the far field to give the single bounce multipath scattering. Double bounce multipath scattering was found by applying physical optics to the incident energy on the front face, radiating the resulting current toward the crest, finding the energy scattered back to the front face using the bistatic crest scattering pattern, again applying physical optics on the front face, and radiating that current to the far field. Distributed surface scattering from the small-scale roughness on the front face of the wave was found using the standard two-scale model (Brown, *IEEE Trans. Antennas Propagat.*, **AP-26**, 472-482). The small-scale and large-scale roughnesses were separated using a moving average filter. The backscattered fields were found through deterministic application of the Kirchhoff approximation and perturbation integrals of Brown to the large-scale and small-scale roughnesses respectively. The complete wave scattering cross-section was then found through coherent addition of the direct crest backscattered field, the multipath field (both single and double bounce), and distributed-surface (two-scale) backscatter from the front face.

The application the three-part mode to the 10 GHz scattering from the single sample of the rough surface shown in Figure 2 is shown in Figure 3. The solid line shows the reference scattering found by applying the MM/GTD approach to the complete roughened wave. The dashed line shows the modeled scattering. Excellent agreement is achieved overall. Figure 4 shows the average cross-sections found by averaging the scattering from 32 random roughness samples (32 Monte-Carlo runs). The reference "exact" cross-sections were again found by applying the MM/GTD approach to the full rough surfaces. Excellent agreement was again achieved. Further analysis of the scattering mechanism showed that the incoherent cross-section resulted from changes in the multipath due to the large-scale random roughness at horizontal polarization (HH). Bragg scattering from the small-scale roughness was insignificant. At vertical polarization (VV), however, the Bragg scattering is much more significant, while the multipath scattering is attenuated by the Brewester angle damping effect proposed by Trizna (*IEEE Trans. Geosci. Remote Sensing,* **35**,1232-1244, 1997). The incoherent cross-section therefore is due to the small-scale roughness at vertical polarization. The coherent cross-section mimics the direct crest scattering at both polarizations.

The results of the 2-D multipath scattering study are fully documented in West and Zhao (*IEEE Trans. Geosci. Remote Sens.*, **40**, 583-592, 2002).

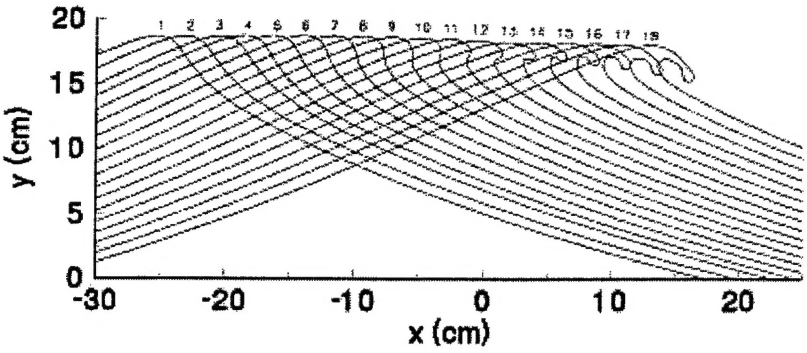

Figure 1 Longtank wave profiles.

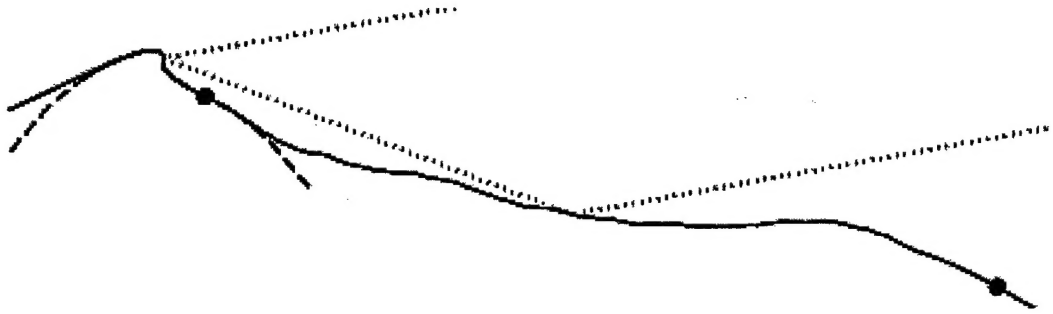

Figure 2 Longtank wave profile 9 with roughened front face. The long-dashed line shows the isolated-crest profile used to find the crest scattering, and the dotted line shows a single backscattering multipath.

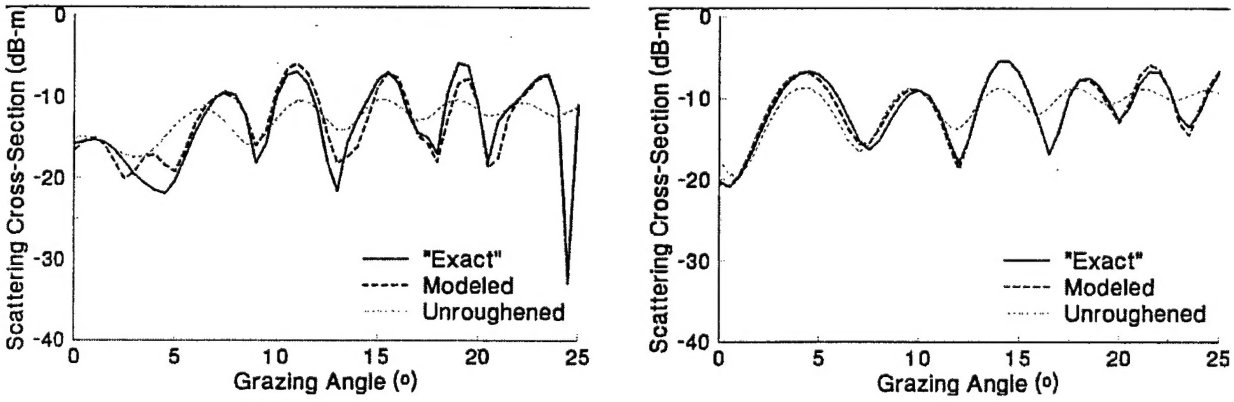

a) HH response.

b) VV response.

Figure 3. Scattering from roughened surface 9. The horizontal axis is the illumination incidence angle (from vertical) and the vertical axis is the scattering cross-section in dB. The solid line gives the exact MM/GTD response and the starred line is the modeled response.

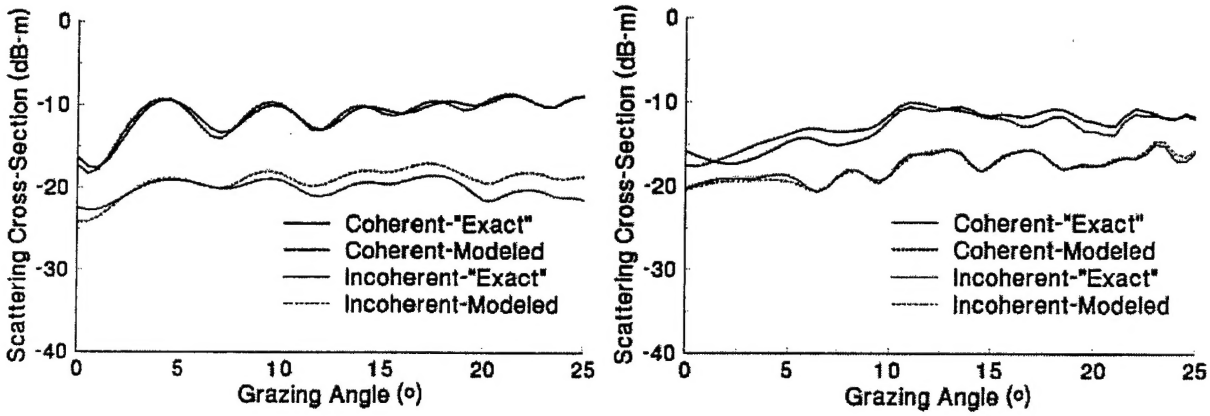

a) HH response.

b) VV response.

Figure 4 Coherent and incoherent scattering cross-sections after averaging of scattering from 32 samples of random roughness in Figure 2.

2-D Crest Scatter

Specular Reflection

The above multipath analysis relied upon direct numerical calculation of the crest scattering using the computationally inefficient MM/GTD approach. A study was performed to examine an efficient model-based method to predict the crest scattering. Figure 5 shows an expanded view of the wave 9 isolated-crest profile. Wave 9 appears at the middle of the breaking sequence, and the jet is just beginning to form. At small grazing illumination angles with illumination from the right, the forming jet feature will present two reflecting faces to the radar, one on the convex section that eventually forms the jet and one on the convave section below that later evolves into the cavity region under the jet. These two points are joined at an inflection point that is marked by the dot in the figure. Energy diffracts from the inflection point due to a reflection shadow boundary. The radii of curvature of the two reflecting surfaces are smaller than a wavelength, so the standard geometrical optics (GO) model is unable to accurately predict the reflected fields. However, a correction factor introduced by Voltmer (PhD Thesis, The Ohio State University, 1970), termed extended geometrical optics (EGO) here, proved effective. EGO introduces a correction factor that is multiplied to the standard GO to extend its accuracy to smaller radii reflection points. The correction affects both the phase and magnitude of the signal, and is different for the two polarizations. The predicted vertically and horizontally polarized backscatter therefore differ.

The scattering from the isolated-crest LONGTANK waves calculated using EGO is shown in Figure 6. The frequency was again 10 GHz, and the grazing illumination angle was 10°. EGO was used to find the directly reflected signal from the convex and concave surface sections. An EGO-corrected diffraction coefficient found from the geometrical theory of diffraction (GTD) was used to find the diffraction from the inflection point. The reference "exact" scattering

was again found using MM/GTD. Prior to wave 8, no specular reflection points appear on the crest. The backscattering is therefore entirely due to diffraction from the inflection point. The vertically polarized backscatter (VV) exceeds that at horizontal polarization (HH) by a small amount here. The scattering is accurately predicted by the EGO-corrected GTD diffraction coefficient. Reflection points appear as the wave begins to overturn. The HH backscattering continues to increase after this point. However, the VV scattering begins to decrease, resulting in a deep null at wave 12. This behavior is predicted by EGO through wave 12. This represents a single-scatter mechanism that leads to a large super event (HH > VV). Because the signs of the surface curvature are different at the two reflection points, the phases of the VV EGO corrections lead to destructive interference between the two reflected signals, giving the deep null. At HH the phase corrections are different, giving constructive interference. Beyond wave 12 the surface curvatures are so small compared to the wavelength that not even EGO can yield realistic responses.

The application of the EGO model to the numerically generated LONGTANK wave profiles is fully documented in West (*IEEE Trans. Geosci. Remote Sensing,* **40**, 523-526, 2002).

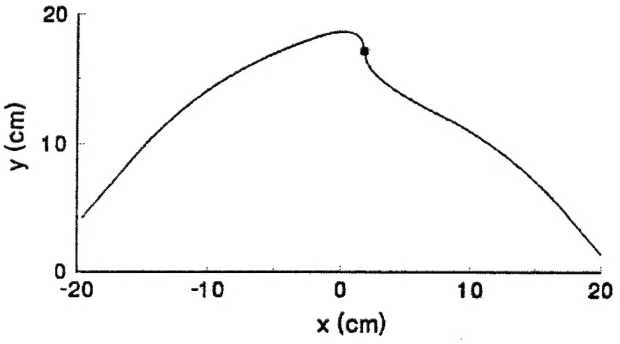

Figure 5. Isolated-crest profile derived from LONGTANK wave 9.

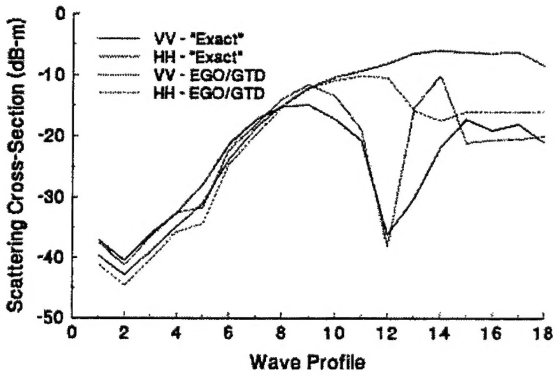

Figure 6. EGO model of scattering from Figure 5 surface.

The EGO scattering model was also applied to plunging breaking wave crest profiles that were directly measured in the University of Maryland wave tank. The individually measured profiles (corresponding to individual frames of the measurement video) were stacked vertically to form Figure 7. Two overturnings occur in the time history. The first is centered at 330 ms and the second is centered at 425 ms. The 10 GHz backscattering from the wave at 10° grazing found using MM/GTD is shown in Figure 8. Nulls appear in the VV scattering during both overturnings while relative maxima occur in the HH signals at the same time. This behavior is quite similar to that calculated with the numerically generated LONGTANK waves.

The EGO treatment of several profiles from Figure 7 is shown in Figure 9. Part a of the figure shows three sample profiles selected from the time period of the first overturning. Part b shows the corresponding EGO analysis. The reference MM/GTD scattering is also shown. The first profile is taken before the jet forms. The scattering is fully diffractive at that point, and EGO-corrected GTD gives a good prediction of the scattering at that time. The jet is well defined

in the second profile. Here a super event has formed, with HH backscattering exceeding VV by up to 10 dB at some grazing angles. EGO gives an overall accurate prediction of the HH to VV ratio, although the VV relative minimum is slightly misrepresented. (The two EGO responses correspond to slightly different radii of curvature used at the reflection points). The jet has fully formed in the third profile, giving a convcave reflection point with a very small radius of curvature (less than 1/5 of a wavelength). A sharp null appears at 12° grazing, giving a very large magnitude. Despite the small radius, EGO again gives a reasonable overall prediction of the HH/VV ratio. The depth of the predicted VV null depends strongly on the exact radius used, however, as shown by the three differing EGO responses.

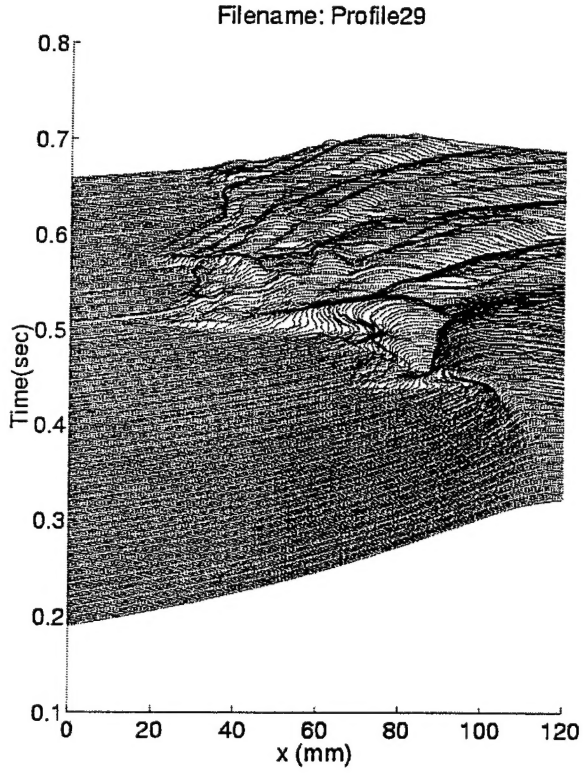

Figure 7 Measured plunging breaker wave.

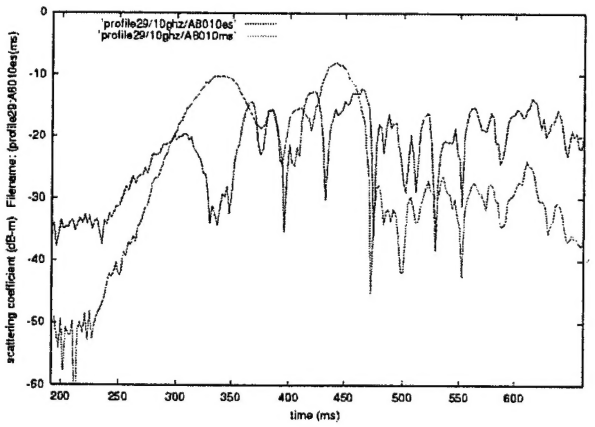

Figure 8 10 GHz backscattering from plunging breaker at 10 degrees grazing. The solid line is VV and the dotted line is HH.

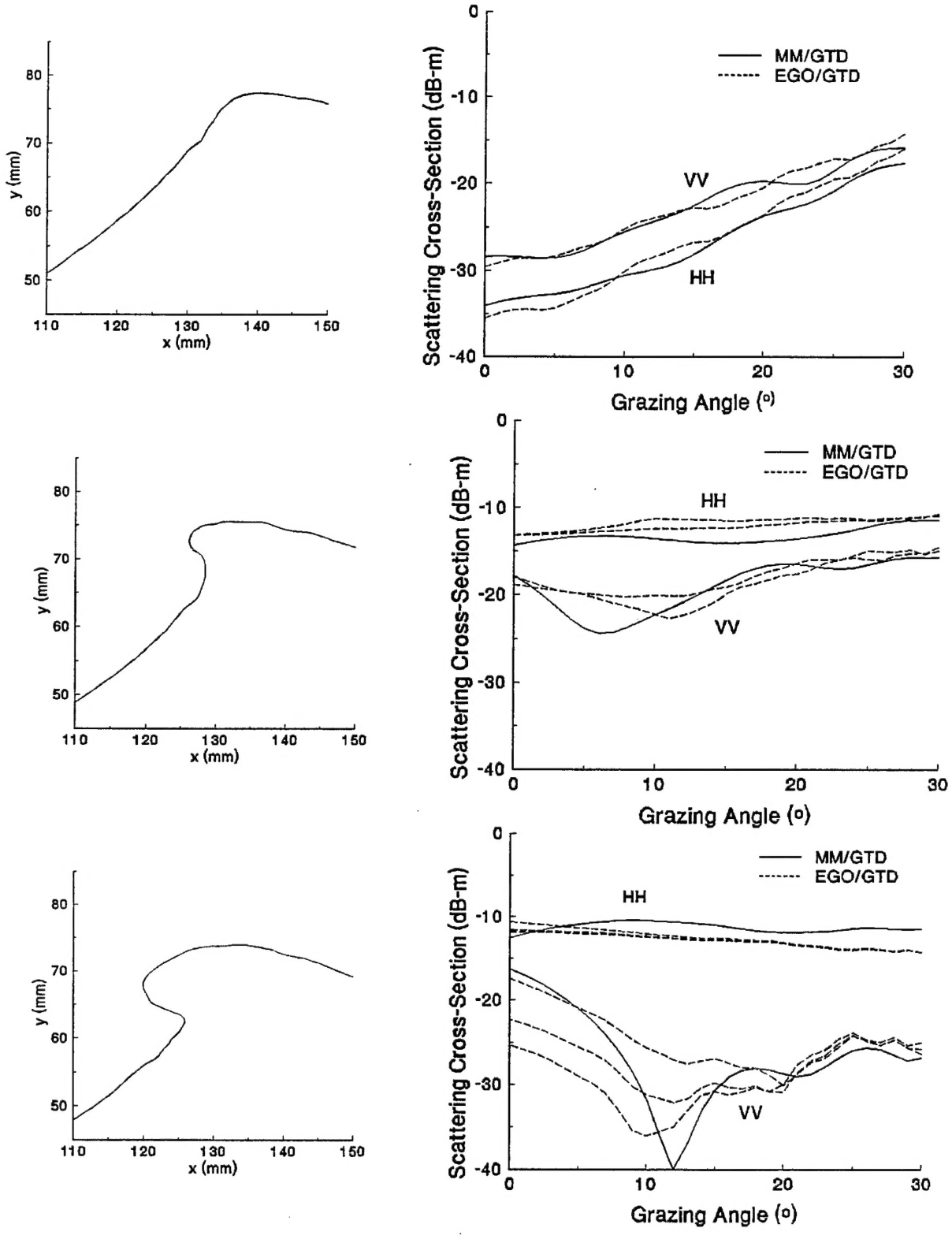

a) Measured crests.

b) Calculated scattering.

Figure 9. EGO analysis of scattering from measured plunging breaker crests.

Distributed-Surface Scatter

In recently published work (West, *Radio Science,* **37,** 7-1—7-12, 2002), the two-scale scattering model (TSM) was applied to the measured low-energy spilling-breaker time history in shown in Figure 10. It was demonstrated that while TSM provides an excellent prediction of the scattering from individual 2-D profiles at moderate grazing angles, it loses accuracy at small grazing. The results are also dependent upon the wave-number threshold used to separate the large-scale and small-scale roughness components. The second-order small-slope approximation (SSA) (Voronovich, *Wave Scattering from Rough Surfaces,* 1999) was therefore considered as an alternative to TSM for LGA scattering from distributed surface roughness. The results at 40° grazing are shown in Figure 9. Excellent agreement is achieved with both TSM and SSA at the times after breaking has begun. However, the SSA results do not depend upon the choice of a scale-separation threshold. The results at 10° grazing are shown in Figure 9. At vertical polarization, TSM is somewhat more accurate than SSA from 350 ms to 500 ms, while SSA shows an advantage after 600 ms. (Prior to 350 ms the wave is overturning, so neither model is expected to be valid. At horizontal polarization, however, SSA significantly underpredicts the backscattering from 350 ms to 600 ms where TSM is accurate. After 600 ms both models are equally accurate. Considering the significant additional computational expense needed to apply second order SSA and its poorer accuracy at horizontal polarization, the use of SSA over TSM at small grazing angles is not recommended.

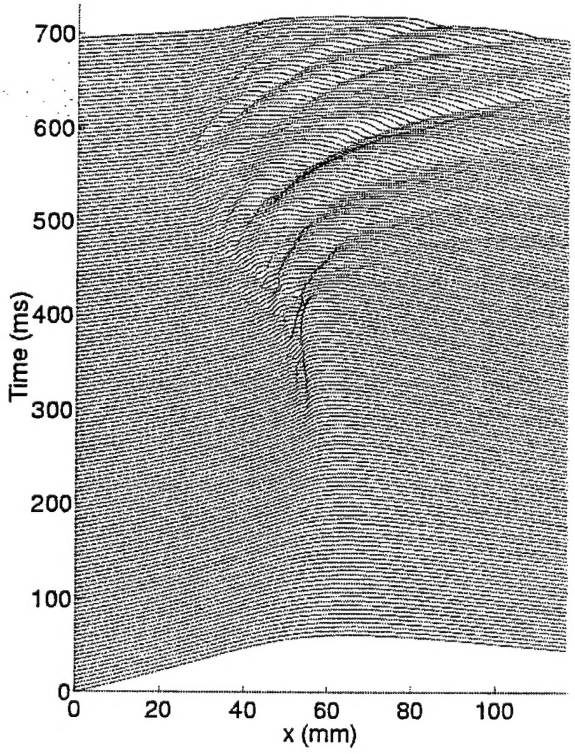

Figure 10. Measured low-energy spilling breaker crest.

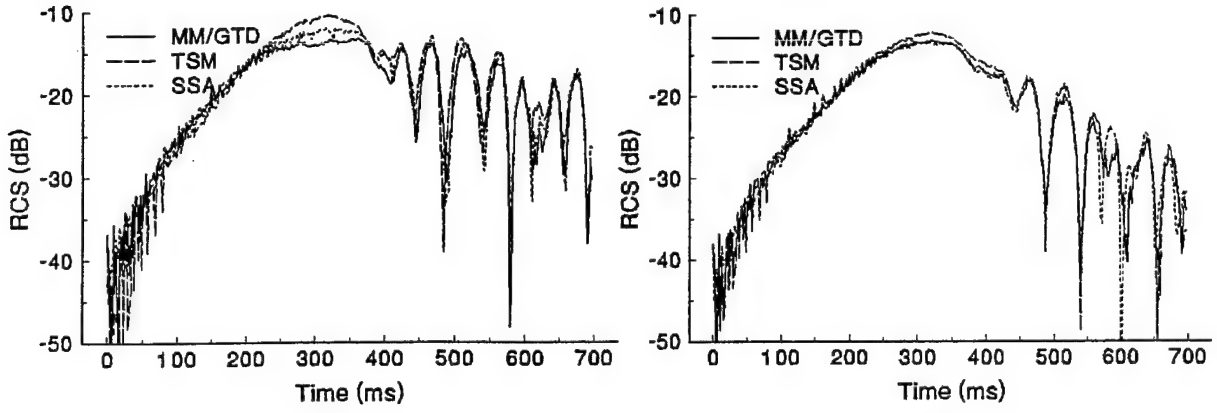

a) VV b) HH

Figure 11. Calculated backscatter from Figure 10 profiles at 40° grazing.

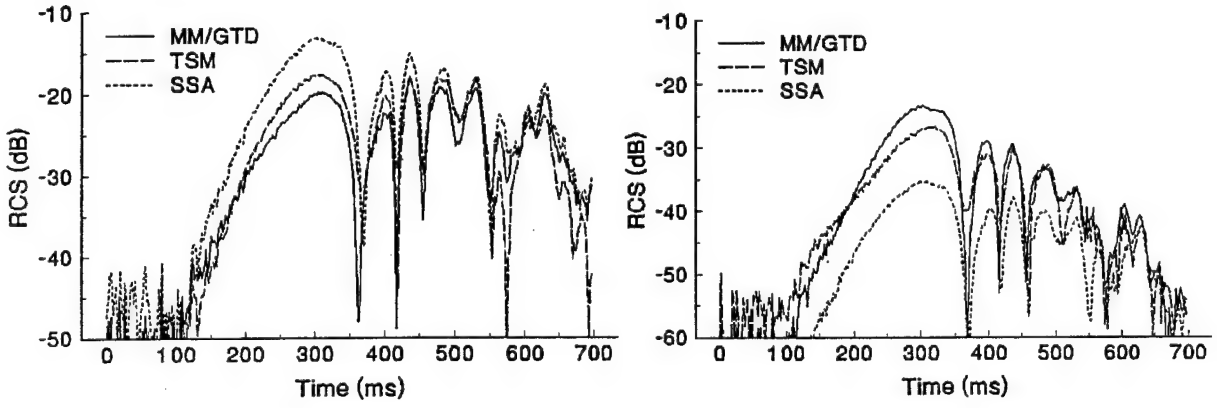

a) VV b) HH

Figure 12. Calculated backscatter from Figure 10 profiles at 10° grazing.

2-D Comparison with Experiment

The MM/GTD approach was applied to another spilling breaker time-history measured in the University of Maryland wave tank. The profile histories are shown in Figure 13a. This spiller is somewhat more energetic that the one shown in Figure 10. These profiles were simultaneously measured with experimental measurements of the radar cross-section performed by Mark Sletten of the Naval Research Laboratory for comparison with the numerical calculations. The 8 GHz scattering cross-sections measured by the NRL radar are shown in Figure 15a. The grazing angle was approximately 12°. A strong super event appears centered at 200 ms, corresponding to the time when the crest includes a steep "bulge" feature. The horizontally polarized (HH) scattering drops rapidly after this time, while the relative maxima in the VV scattering remain approximately constant. The MM/GTD approach was

applied directly to the measured crests. The results are shown in Figure 15b. Overall, the dependence of the numerical and experimental scattering on time are similar. In particular, both show relative maxima at the same times, corresponding to the times when turbulent cells are shed from the crest. However, the HH-to-VV polarization is significantly different.

Two mechanisms that may contribute to the incorrect numerical HH/VV ratio were investigated. The first was the introduction of multipath scattering. In this, the front faces of the individual wave profiles were extended at different depths below the mean water level as shown in Figure 14. The front face extension provides a reflecting surface that introduces multipath scattering from the wave crest that interferes with the direct crest backscatter. The calculated backscattering when the face was extended at the mean water level (the solid line in Figure 14) is shown in Figure 15c. At 0.2 s the HH backscattering has increased and the VV backscattering has decreased, giving a large HH/VV ratio. However, it is still considerably less than the experimentally measured ratio. At later times the scattering is from distributed surface roughness rather than quasi-specular reflection from the overturning crest, so the multipath is much smaller and the scattering is essentially unaffected. Use of the other front face extensions in Figure 14 gave different HH/VV ratios. The other mechanism considered was near-field antenna pattern effects. The physical constraints of the experimental setup required the radar antennas be operated somewhat within the near field range. The near-field amplitude pattern of the radar antennas was therefore measured at the Naval Research Laboratory and incorporated into the numerical calculations. It was found that the HH/VV ratio increased as the antenna pattern was aimed over the top of the wave crest rather than exactly on the crest due to differing HH and VV beamwidths. The results with the pattern centered 12 cm over the wave peak are shown in Figure 15d. The HH/VV ratio is again increased, but not sufficiently to match the experimental results. It is likely that both mechanisms contribute to large HH/VV experimentally measured. As shown in previous work (West, *IEEE Trans. Geosci. Remote Sensing*, **40**, 583-92), the multipath interference is extremely sensitive to the exact front face profile at LGA, so without detailed measurement of the front face it is impossible to predict exactly the overall effects of this mechanism. Moreover, lack of the phase of the antenna pattern similarly limits the accuracy of the pattern-effect study. Both of these issues will be addressed in a series of experiments scheduled at the University of Maryland wavetank in the Spring of 2003.

The experimental scattering from the plunging breaker wave shown in Figure 13b was also compared with the numerical calculations. The results are shown in Figure 16. Again, the HH/VV polarization ratio does not agree between the experimental and numerical results. However, the overall features of the responses are similar. In particular, both show large multiple responses to both the initial jet formation and the subsequent "splash-up" responses to the jet impact that leads to another overturning. Moreover, both the numerical and experimental results show HH maximum responses at ~210 ms, with nulls appearing at VV at the same time. This is similar to the behavior observed in Figure 6 with the ideal LONGTANK numerical wave. This represents the first experimental demonstration of the VV null predicted in the 2-D numerical results.

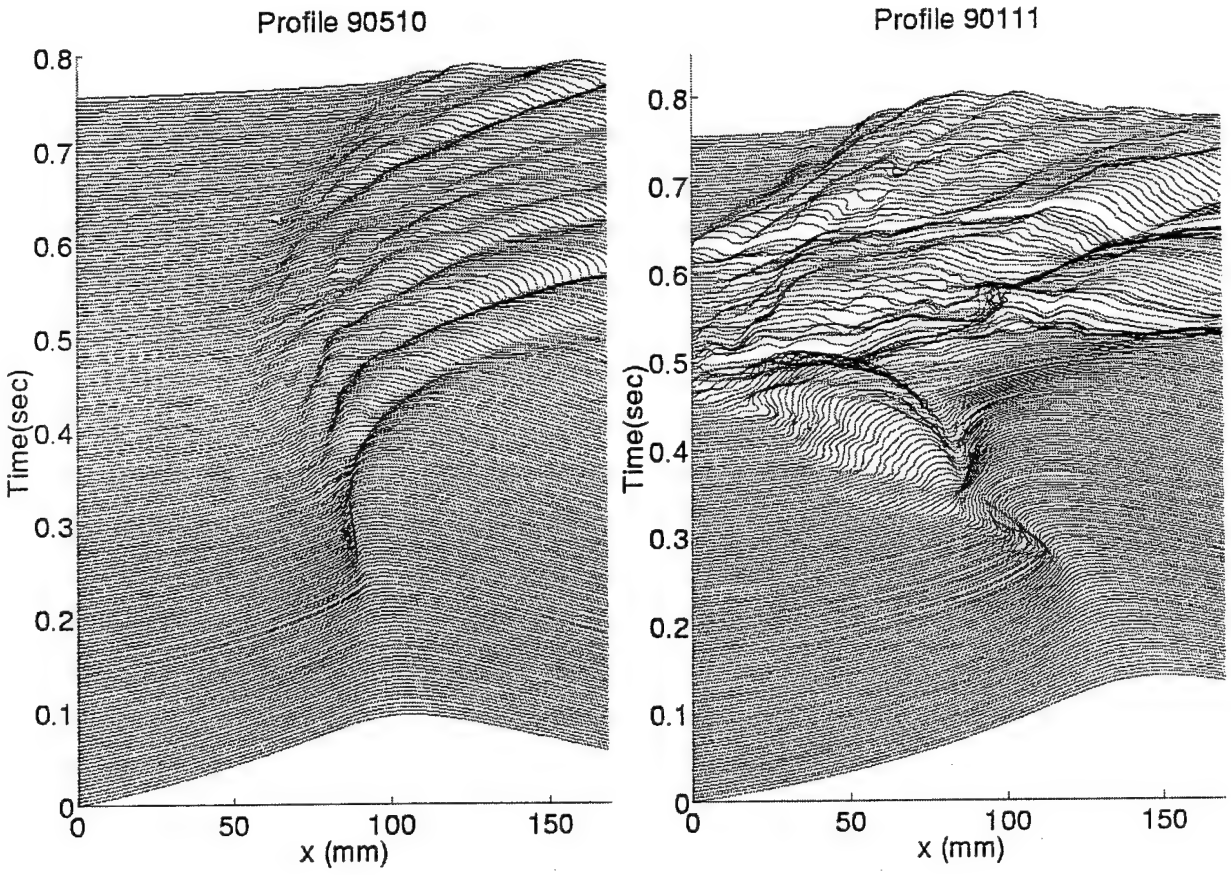

Figure 13. Measured time history of crests of breaking water waves. a) Spilling. b) Plunging.

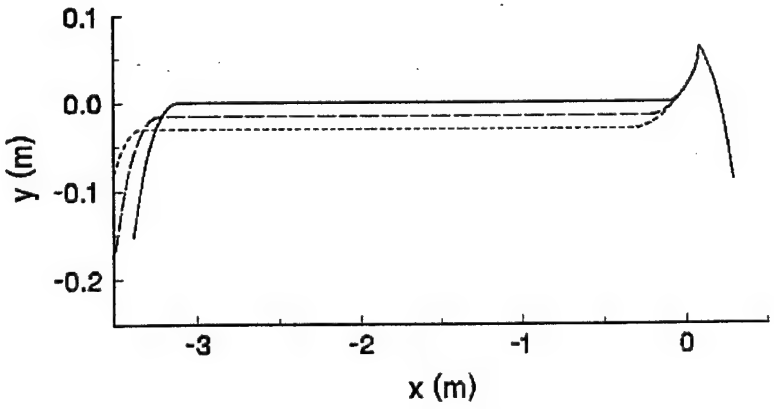

Figure 14. Extended wave profile front faces.

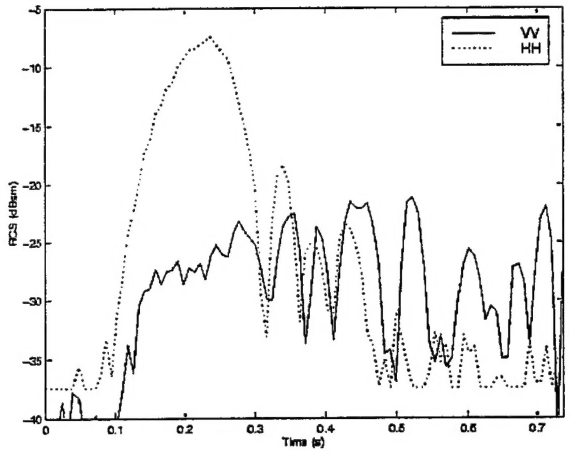

a) Experimentally measured in wavetank.

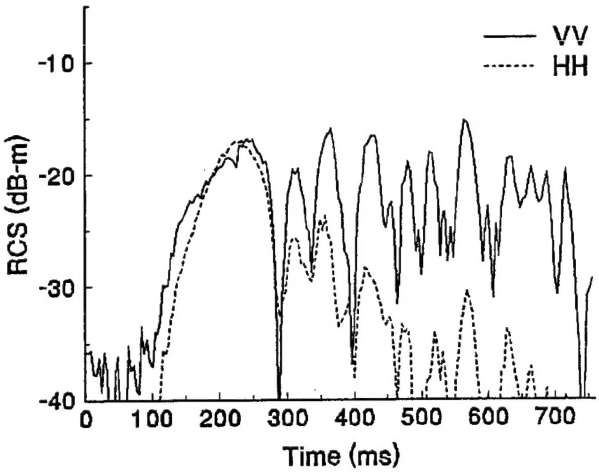

b) Numerically calculated from crests alone.

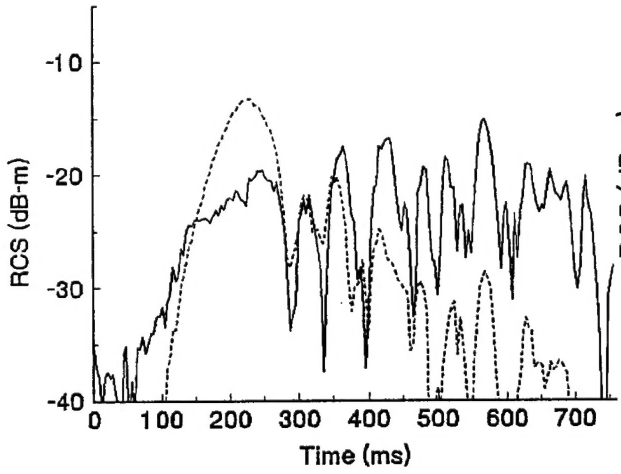

c) With front face extension of Figure 14.

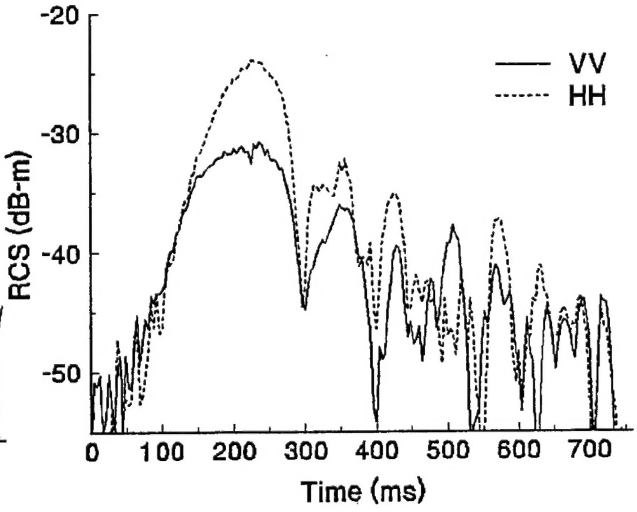

d) With misaimed antenna.

Figure 15. Calculated scattering from profiles of Figure 13a.

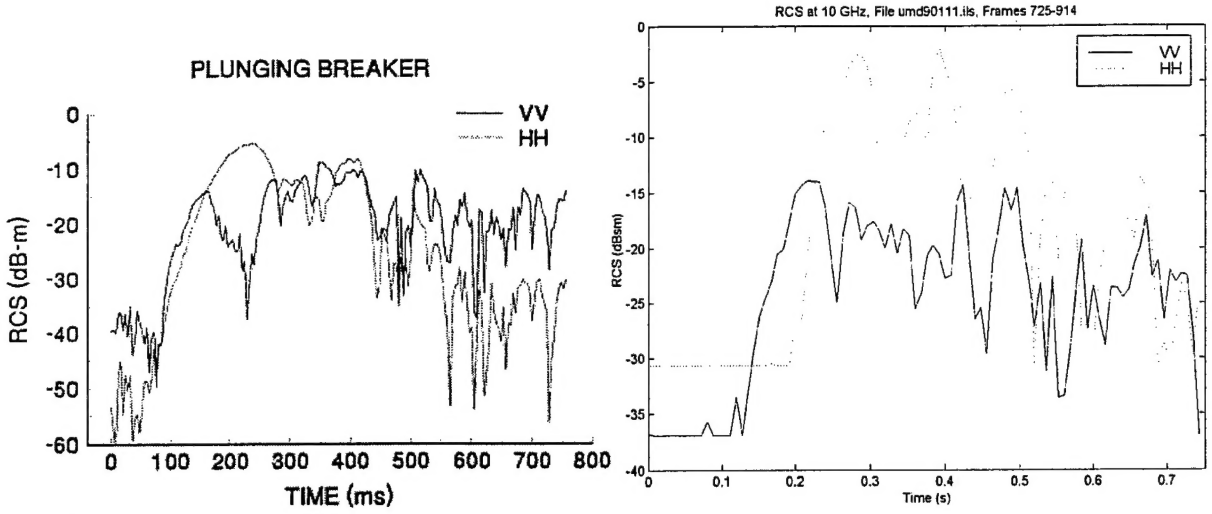

a) Numerical. B) Experimental.

Figure 16. Scattering from measured plunging breaker.

3-D Numerical Scattering Code

The multilevel fast multipole algorithm (MLFMA) numerical scattering technique was implemented to find the scattering from arbitary surfaces that are rough in two dimensions. The algorithm was implemented using object-oriented methods, allowing an arbitrary number of levels to be used. This allows extremely large systems to be considered. The method was implemented using impedance boundary conditions to represent the finite conductivity of sea water. Diffraction from the artificial edges introduced by truncating the surface to fit within finite computer resources is controlled using a resistive edge loading that was previously developed for two-dimensional surfaces (Zhao and West, *Proceedings of the 2002 International Symposium on Antennas and Propagation,* San Antonio, TX, 264-267.) It has been parallelized to allow the sparse matrix to be distributed across multiple processors, and an incomplete LU factorization of the sparse matrix is used as a preconditioner.

The MLMFA implementation was applied to the test surface shown in Figure 17. This 3-D surface was formed by azimuthally extending the 2-D profile 9 of the LONGTANK wave series. The calculated scattering at both VV and HH polarizations is shown in Figure 18. Also shown is reference scattering found from the original 2-D profile 9 and converted to a 3-D cross-section from the equivalent width of the surface. The 3-D FMM calculations agree with the reference 2-D results to within 1 dB under most conditions. The only exception is in the VV null at 10^{o}, where the error reaches 1.5 dB. This is acceptable performance, showing that the FMM results can be used for the crest scattering for a model-based 3-D approach for backscattering from breaking water waves.

A 3-D spilling breaker crest was artificially formed by azimuthally aligning the individually measured 2-D profiles of Figure 10. The final wave crest, including extensions needed for the application of the resistive loading to avoid edge diffraction, is shown in Figure 19. The calculated 10 GHz scattering at both VV and HH polarization is shown in Figure 20. Also shown is the reference scattering found by applying the 2-D MM/GTD technique to the

individual profiles and adding the results coherently to yield an equivalent 3-D cross-section. Very good agreement is achieved between the two cases. This indicates that the steep section of the crest that gives a coherent reflector dominates the backscatter. This was further demonstrated by forming a truncated wave crest that eliminated the steep section in Zhao (Ph.D. Dissertation, Oklahoma State University, December 2002). A two-scale treatment of the truncated wave scattering has recently been documented by Zhao (Ph.D. dissertation, Oklahoma State University, December 2002).

A 3-D breaking profile was also formed from the first overturning of the measured 2-D profile of Figure 7. The resulting wave crest is shown in Figure 21. Five manually identified reflection points that were used in a 3-D EGO analysis are labeled on the crest. The calculated scattering at 10 GHz is shown in Figure 22. In this case, the HH scattering has an approximately constant cross-section at all grazing angles considered. The VV scattering on the other hand shows a deep null at 5° grazing, indicating that reflections from two or more points are destructively interfering. The EGO analysis is able to predict this null while simultaneously providing a decent prediction of the HH scattering. However, it should be noted that achieving this degree of accuracy required that the parameters of the reflection points (the radii of curvature in the along- and across-look directions) be manipulated manually. These results should therefore be considered preliminary. On the other hand, this result does show that EGO has the potential to predict important features of 3-D crest reflection. A follow-on study to develop an automated procedure to find the relevant curvatures with more realistic wave shapes is now underway.

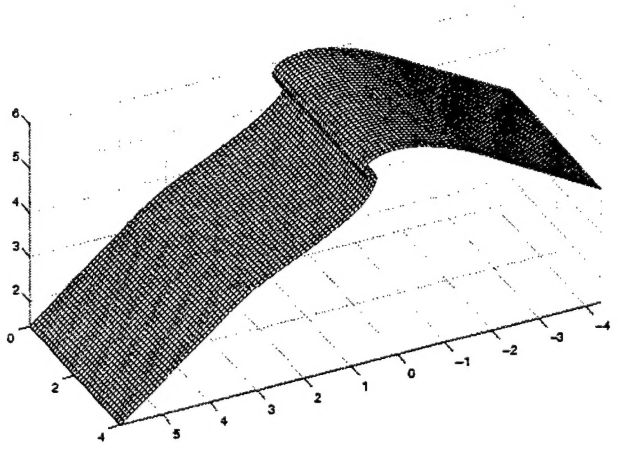

Figure 17. 3-D breaking wave crest formed by extending a numerically generated 2-D crest azimuthally. The dimensions are electromagnetic wavelengths at 10 GHz (3 cm).

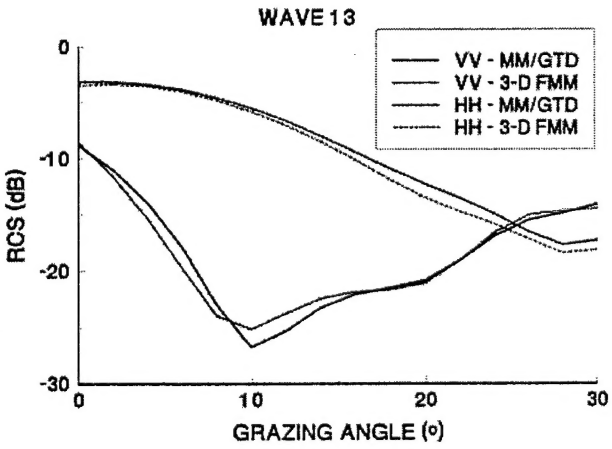

Figure 18. Calculated scattering from Profile in Figure 17.

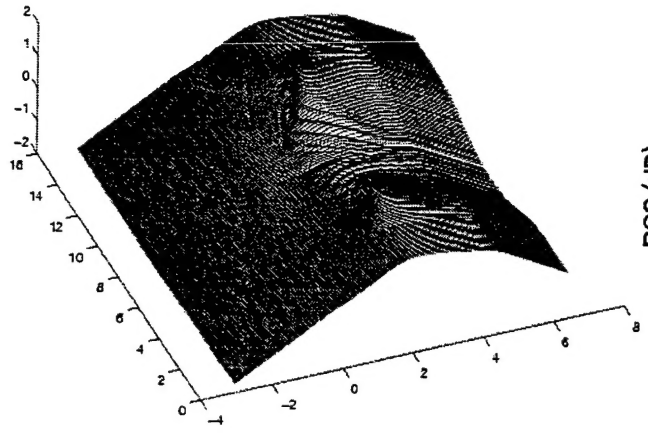

Figure 19. Three dimensional breaking crest formed from measured 2-D time history.

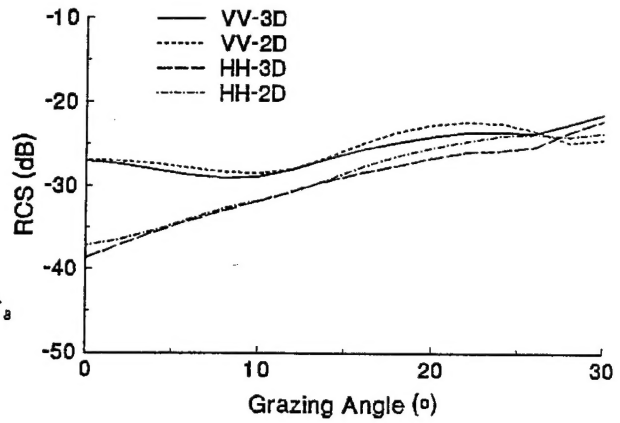

Figure 20. Calculated scattering from spilling breaker of Figure 18.

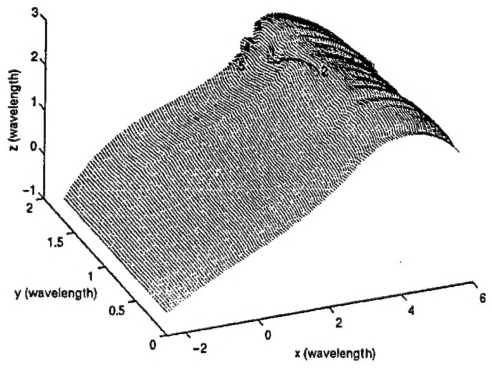

Figure 21. 3-D plunging crest.

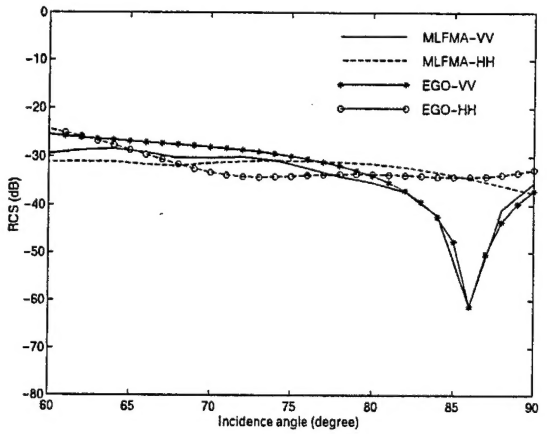

Figure 22. Scattering from 3-D plunging crest.